

Fast-Time Clutter Suppression in mm-Wave Low-IF FMCW Radar for Fast-Moving Objects

Christopher Allen¹, Levi Goodman¹, Shannon D. Blunt¹, and David Wikner²

¹Radar Systems Lab, University of Kansas, Lawrence, KS

²Sensors and Electron Devices Directorate, US Army Research Laboratory, Adelphi, MD

Abstract— A dual-DDS-based, mm-wave, heterodyne, FMCW radar with a 108-GHz center frequency, a 600-MHz bandwidth, and a 3-MHz IF was used to characterize backscatter from static clutter and a small, fast-moving target. Employing a symmetric triangular frequency-vs-time FMCW waveform with 500- μ s up-chirp and down-chirp durations, signals from a reusable paintball (reball) with a radial velocity of about 90 m/s were measured in an indoor, clutter-rich environment over intervals of \sim 100-ms. Unambiguous estimation of the reball's range and radial velocity were derived from observations made during both the up-chirp and down-chirp observations. Specifically, when the reball's echo signal was obscured or degraded by coincident clutter (e.g. during down-chirp), estimates of its amplitude characteristics were obtained from measurements when the reball and clutter were spectrally separable (during up-chirp). Consequently, it is demonstrated that the clutter in this context can be suppressed by more than 25 dB.

I. INTRODUCTION

Frequency-modulated, continuous-wave (FMCW) radars operating at mm-wave frequencies can offer fine spatial resolution and high Doppler sensitivity for sensing targets both nearby and at modest distances. Their short operating wavelength enables the use of compact-sized antennas making them suitable for operation on mobile platforms. Recent published applications address FMCW mm-wave radars for small UAV characterization [1] and automotive safety systems [2,3] such as adaptive cruise control, collision warning, and collision avoidance [2]. Such applications require the ability to distinguish between signals from static and moving targets. Thus a means of clutter suppression is needed [4].

One of the key benefits afforded by FMCW radars is the ability to use wide bandwidth signals to achieve fine range resolution through analog-domain dechirping. This process involves mixing the received signal with the transmitted signal so that the post-mixer intermediate frequency (IF) signal has a modest bandwidth, thus avoiding the need for high-performance signal acquisition and the corresponding enormous data volumes. Such a system is termed homodyne when the IF signal is centered at 0 Hz (DC). Due to signal aliasing about DC the ability to distinguish between positive and negative frequency mixing products is lost unless complex sampling techniques are employed.

In contrast, a system is termed heterodyne if the IF signal is not centered at DC. To realize a heterodyne FMCW radar [5] requires an alternative architecture wherein dechirping of the received echo signal is performed not with the actual transmitted signal but instead with a reference signal that is a frequency-shifted version of the transmitted signal. This

approach shifts the IF away from DC and thus provides explicit separation of positive and negative frequency mixing products. Reference signal generation can take a variety of methods. For example, [5] produces the transmit and reference waveform signals using sweeping voltage-controlled oscillators (VCOs), while direct-digital synthesizers (DDSs) were used in [6] to provide precise and repeatable waveforms.

From an application perspective, FMCW radars can provide mobile platforms with situational awareness regarding potential nearby static obstacles as well as moving hazards. The ability to detect and report both static and moving objects is relevant to both ground-based platforms (e.g. automobiles [2]) and to airborne platforms (e.g. small UAVs [7]). When the moving objects persist in the radar's field of view over a coherent-processing interval (CPI) two-dimensional spectral processing (e.g. 2-D FFT) can reliably provide information on both static and moving targets. For fast-moving objects that may be observable only during a small fraction of the CPI and can likewise introduce significant range-walking, the 2-D FFT approach may not suffice. For such cases a different signal processing approach may be needed.

In this paper we report findings from an FMCW heterodyne radar architecture at W-band (108 GHz) to evaluate the challenges of detecting and characterizing a small, fast-moving object within an environment of (mostly) static clutter. During the course of this investigation various novel techniques for suppressing static clutter to reveal the fast-mover's echo were applied and a successful method is presented here. The following describes the test setup, experimental measurements, and the result of applying this clutter cancellation technique. Another approach is also demonstrated in companion paper [8].

II. SYSTEM DESCRIPTION

A DDS-based, mm-wave FMCW radar system was developed around the Virginia Diodes Inc. integrated amplifier/multiplier chain (WR10AMC-I) W-band transmitter module and their integrated mixer/amplifier/multiplier chain (WR10MixAMC-I) W-band receiver module [9]. Both modules have integrated $6\times$ frequency multiplication and therefore the useful input frequency range of 12.5 to 18.33 GHz provides the W-band frequency range of 75 GHz to 110 GHz. Likewise, a waveform bandwidth of 100 MHz produces a mm-wave bandwidth of 600 MHz.

Figure 1 illustrates the system block diagram. All oscillators (DDS clock, LO #1, and LO #2) are phase locked and the two DDSs are triggered simultaneously. Additional

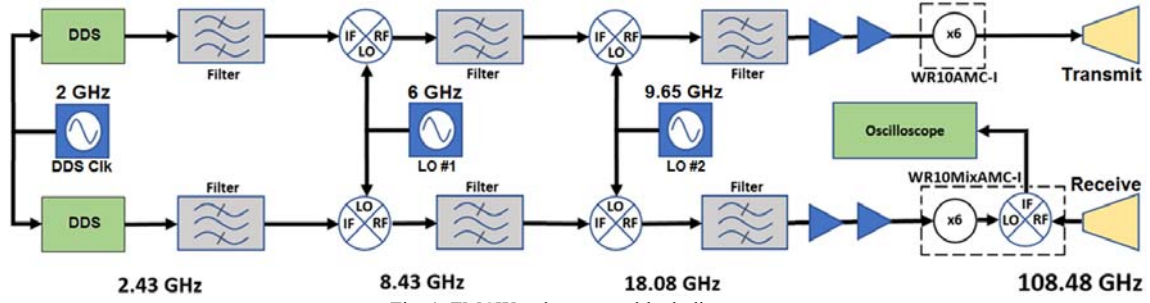


Fig. 1. FMCW radar system block diagram.

system details are available in [10].

The FMCW radar uses triangular waveforms as depicted in Fig. 2. The DDSs are programmed to produce baseband triangular linear-FM (chirp) waveforms from which the transmitted and reference signals are derived. These waveforms have in common the up-chirp and down-chirp waveform durations, τ_{up} and τ_{dn} , which need not be identical, and the overall swept bandwidth B . The center frequencies of these waveforms are offset by f_o to support heterodyne operation.

In addition to the transmit and reference waveforms, Fig. 2 also illustrates two received waveforms; one (red trace) is a time-delayed version of the transmitted waveform (i.e. without motion there is no Doppler frequency shift, $f_D = 0$), while the other is both time-delayed and Doppler frequency-shifted (purple trace). In both cases, point targets (scatterers) reside at the same range from the radar.

The waveform for the illustrated moving target in Fig. 2 has a vertical shift by f_D , representing a negative Doppler frequency shift. Thus the range R from the radar to the target is increasing during the observation time. The horizontal shift T of the received signal relative to the transmitted signal represents the time delay corresponding to the time-of-flight from the radar to the scatterer and back to the radar.

Also shown in Fig. 2 are the frequency components contributing to the measured beat frequencies for these two targets, where a target's beat frequency results from mixing the received waveform with the reference waveform. During the up-chirp portion of the transmitted waveform the beat

frequency f_{b_up} depends on a range-related frequency shift f_{R_up} , the Doppler frequency shift f_D , and the offset frequency f_o . Similarly, the beat frequency during the down-chirp portion of the waveform f_{b_dn} depends on a range-dependent frequency shift f_{R_dn} , the Doppler frequency shift f_D , and the offset frequency f_o . Assuming a constant target velocity during the observation time, the f_D and f_o terms will be identical in f_{b_up} and f_{b_dn} . However the range-dependent frequency shift terms will not be the same due to different slopes for the up-chirp and down-chirp frequency versus time characteristics.

Figure 3 illustrates the relative beat frequencies for the stationary and moving targets depicted in Fig. 2. The relative

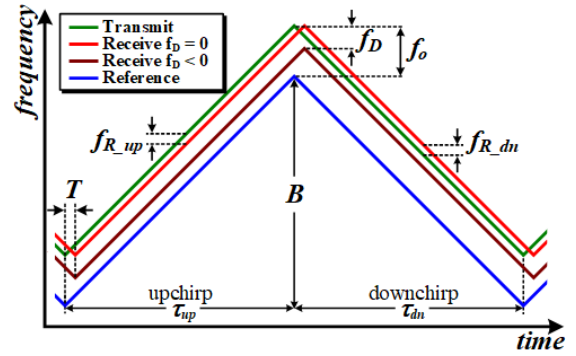


Fig. 2. Frequency-time diagram of the triangular FMCW radar waveform showing the transmitted, received, and reference instantaneous frequencies as well as range-dependent beat frequencies for both a static point target, i.e. no Doppler frequency shift ($f_D = 0$), and a point target moving away from the radar, i.e. a negative Doppler frequency shift ($f_D \neq 0$).

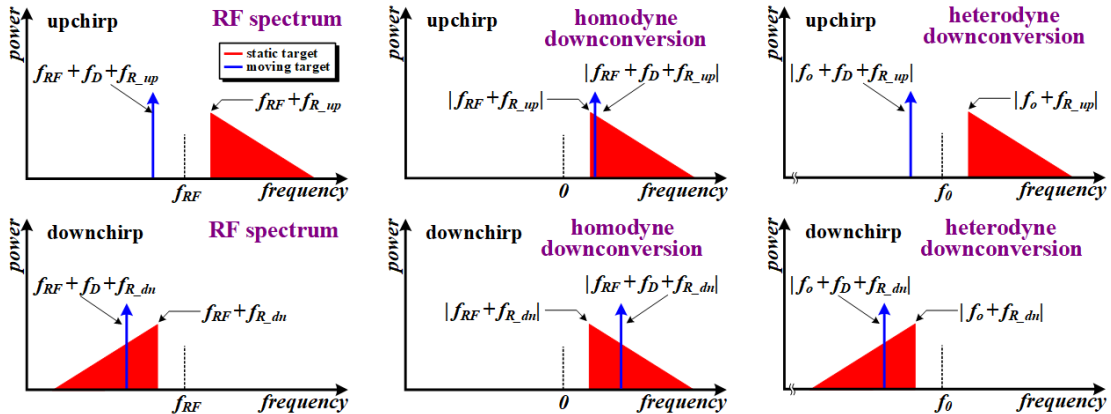


Fig. 3. Radar signal spectra for a point target moving away from radar and extended static clutter received during (top) the up-chirp and (bottom) down-chirp portions of the waveform. The left column depicts the RF (mm-wave) signal spectra, the center column the spectra after homodyne down-conversion (i.e., $f_o = 0$), while the right column shows the spectra after heterodyne down-conversion.

beat frequencies for extended static scattering (e.g. clutter) and a target moving away from the radar are illustrated separately for up-chirp and down-chirp waveforms as well as for homodyne ($f_o = 0$) and heterodyne receiver configurations. Note that for a homodyne system the moving target's signal is always coincident with the clutter return, while for the heterodyne system the mover is spectrally isolated from the clutter in the up-chirp case yet remains coincident with clutter in the down-chirp case.

The following relationships apply to this configuration:

$$T = 2R/c \quad (1)$$

$$f_D = -2v f_{RF}/c \quad (2)$$

$$f_{R_up} = 2BR/(\tau_{up}c) \quad (3)$$

$$f_{R_dn} = -2BR/(\tau_{dn}c) \quad (4)$$

$$f_{b_up} = f_o + f_D + f_{R_up} \quad (5)$$

$$f_{b_dn} = f_o + f_D + f_{R_dn} \quad (6)$$

where c is the speed of light in the medium, v is the scatterer's radial velocity, and f_{RF} is the radar's center frequency. Note that for targets moving away from the radar, the range-rate $dR/dt > 0$, the velocity $v > 0$, and the Doppler frequency $f_D < 0$.

III. TEST SETUP AND MEASUREMENT RESULTS

The setup for collecting indoor radar data is shown in Fig. 4. The FMCW radar was oriented such that a 3.2" trihedral (RCS ~ 7.7 dBsm) and a 6" trihedral (RCS ~ 18.7 dBsm) were within its field of view at distances of about 4 m and 6 m from the radar, and beyond these was a wall. The moving target was a 0.68"-diameter reusable paintball (reball) that was fired from a paintball gun (nominal muzzle velocity of 200 mph). A standard bedsheet was suspended in front of the wall to absorb the energy of the reball which was **fired away** from the radar's position toward the wall. An infrared sensor mounted on the paintball gun's barrel detects the passage of the reball from the gun's muzzle and sends a trigger signal to the oscilloscope that records the radar's heterodyne output signal. Also captured on the oscilloscope were the strobe signals from the DDSs to identify the endpoints of each chirp sweep.

The results described here were obtained with the following system parameters: 108.48 GHz radar center frequency, 600 MHz chirp bandwidth, 500 μ s up-chirp and



Fig. 4. Diagram of test setup showing the static targets and moving target within the radar's field of view.

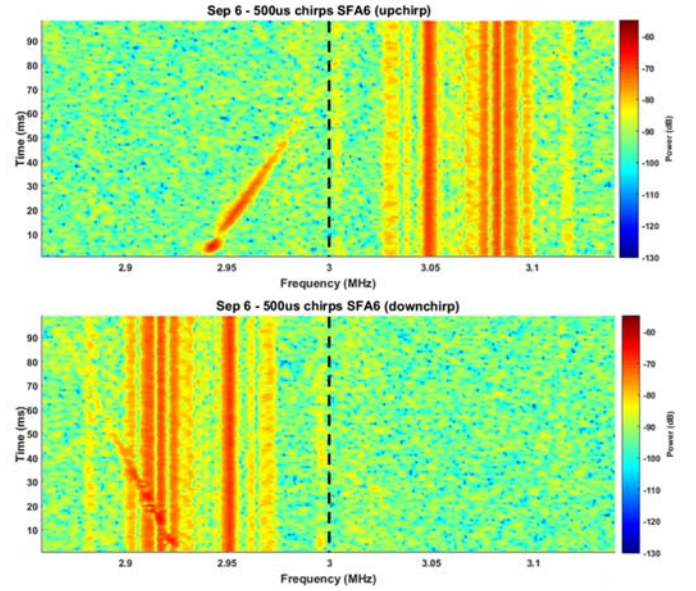


Fig. 5. Spectrograms of radar echo spectra over time showing backscatter from static targets and a reball **fired away** from the radar when illuminated by (top) up-chirp waveforms, and (bottom) down-chirp waveforms.

down-chirp durations, 3 MHz heterodyne offset frequency, 1 to 10 m nominal target range, 90 m/s nominal moving target radial velocity, and ≥ 10 GSa/s oscilloscope sample frequency.

The radar data recorded on the oscilloscope was then processed as follows for each reball shot fired: 1) the data is parsed into segments representing each chirp sweep, noting the timestamp and whether it was an up-chirp or down-chirp waveform; 2) FFTs were performed on these data segments to produce signal spectra records; 3) signal spectra output data were converted to a dB scale and then assembled to form spectrograms as shown in Fig. 5.

The spectrogram pair in Fig. 5 shows sequential scene echo spectra over a 100 ms observation time for up-chirps and down-chirps separately. The beat frequency of the fast-moving reball is below the 3-MHz offset frequency in both cases. The static clutter (from trihedrals, auditorium fixtures and furniture, and the wall) appears above the offset frequency in the up-chirp spectrogram and below the offset frequency in the down-chirp spectrogram. Thus the reball's signature is obscured by the static clutter in an alternating manner. Since the degraded signal-to-clutter ratio in the down-chirp spectrogram complicates estimation of the reball's flight, a technique for suppressing clutter and subsequently enhance detection of this fast-moving object was developed.

A different spectrogram pair shown in Fig. 6 contains results for the case where the reball is **fired toward** the radar from a position in front of the radar. In this case the sheet is suspended in front of the radar so that it does not impact the radar equipment. Since the reball now has a positive Doppler frequency, the reball's echoes appear to the right of the offset frequency and the clutter obscures the reball during up-chirp waveforms. At around 65 ms the character of the reball's signature changes abruptly, which corresponds to when it reaches the sheet and decelerates rapidly. In addition, the

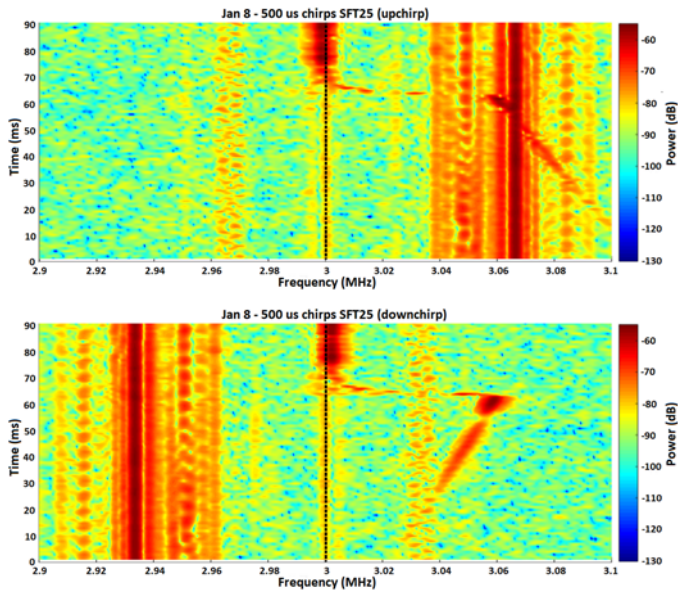


Fig. 6. Spectrograms of radar echo spectra over time showing backscatter from static targets and a reball **fired toward** the radar when illuminated by (top) up-chirp waveforms, and (bottom) down-chirp waveforms.

kinetic energy transferred to the sheet deforms its shape due to vibration, causing its RCS to increase significantly.

IV. CLUTTER SUPPRESSION FOR FAST-MOVING OBJECTS

Several techniques for suppressing the clutter in the down-chirp spectrogram were explored with varying degrees of success. One effective technique involves spectrally folding the up-chirp spectrum to obtain an estimate of the clutter in the down-chirp spectrum to facilitate cancellation. Specifically, the magnitude response of the up-chirp spectrum represents a “clutter only” condition that avoids suppressing the moving target. This magnitude response is combined with the phase response of the down-chirp spectrum (since the folding is not perfect) and is then subtracted from the down-chirp spectrum to reveal the reball response.

Fig.7 illustrates this process when the reball is **fired away** from the radar. Figures 8 and 9 show the results of this

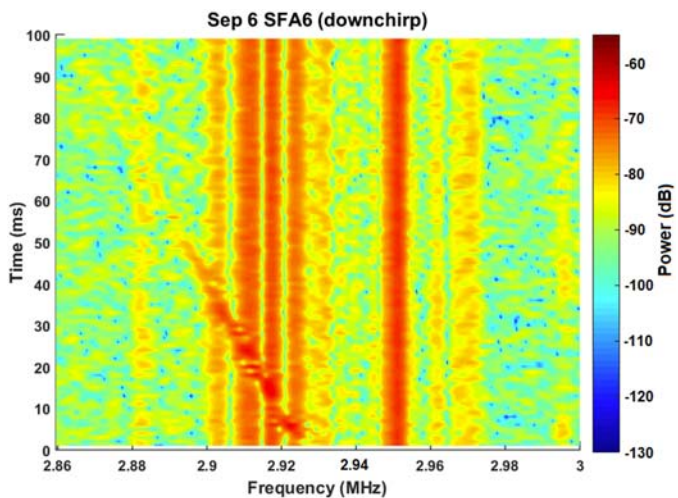


Fig. 8. Down-chirp spectrogram before clutter cancellation (**fired away**).

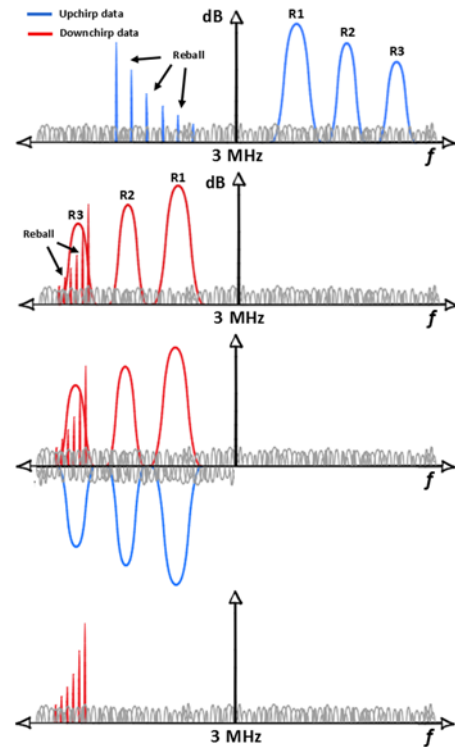


Fig. 7. Illustration of the clutter suppression process where (top) the up-chirp and down-chirp data spectra are parsed for multiple chirp sweeps. Then the up-chirp frequency response is spectrally folded about the offset frequency, albeit with the opposite sign (middle), so that their *summation* suppresses the clutter, leaving only the reball response (bottom).

suppression process for the down-chirp spectrogram (bottom panel of Fig. 5). Here this “fold-and-subtract” technique suppressed the clutter to at least the background noise floor (i.e. by > 25 dB). Moreover, while the eye can clearly see the reball traverse the spectrogram in this case without clutter cancellation (because we recognize the pattern it makes), automated detection and tracking would likely not fare as well. The response in Fig. 9 would thus certainly make it easier to automate detection/tracking.

For the alternative arrangement when the reball is **fired**

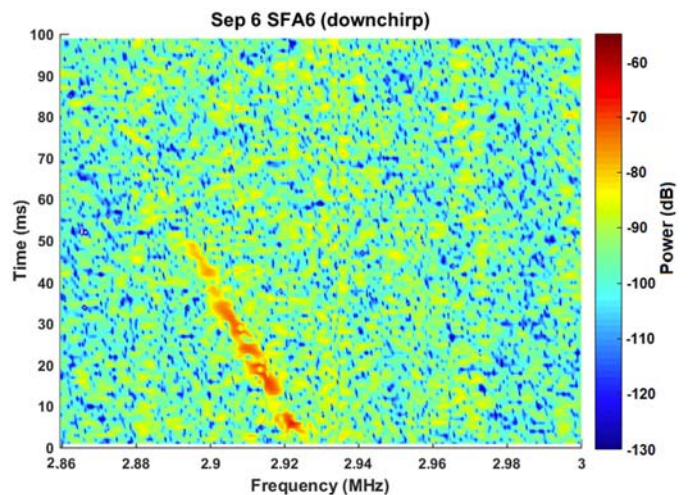


Fig. 9. Down-chirp spectrogram after clutter cancellation (**fired away**).

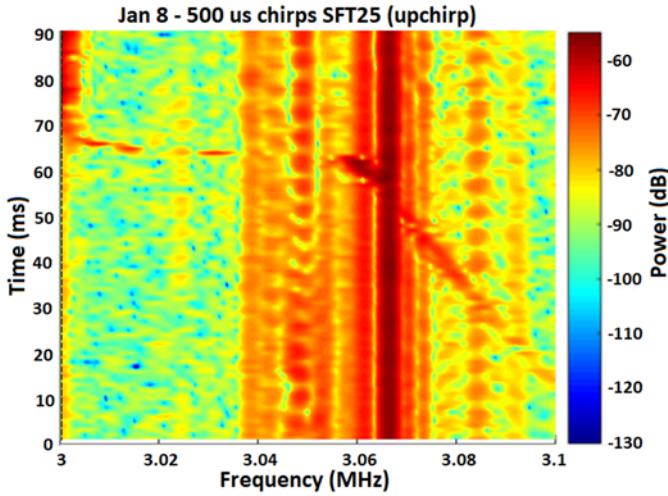


Fig. 10. Up-chirp spectrogram before clutter cancellation (fired toward).

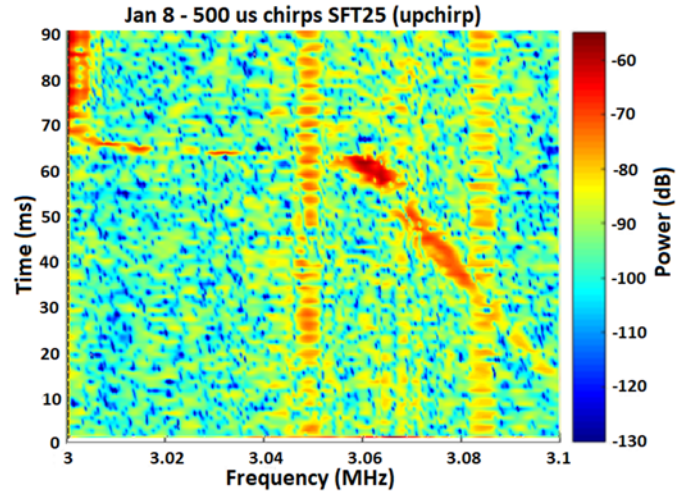


Fig. 11. Up-chirp spectrogram after clutter cancellation (fired toward).

toward the radar, the roles of the up-chirp and down-chirp responses in Fig. 7 are reversed. Figures 10 and 11 illustrate the result when the “fold-and-subtract” technique is applied in this case. We again see that the static clutter has been successfully suppressed, though there is some residual from dynamic clutter that remains. This dynamic clutter may be from nearby ventilation fans that were not operating at the time that the Sep 6 SFA6 data set was collected.

The reball’s beat frequency signal contains information regarding both the range $R(n)$ and radial velocity $v(n)$ over the observation time. Using the up- and down-chirp beat frequency equations from (5) and (6), it is straightforward to solve for these parameters and thereby estimate the trajectory of the fast-moving object.

In this process, a low latency approximation can be made by using three sequential sweeps (e.g. up-, down-, up-chirp), where the beat frequency coincident with the middle sweep is obtained from the mean of the first and last of the three beat frequencies. For example, consider three consecutive reball beat frequency observations ($n = 13, 14, 15$), with observations 13 and 15 from down-chirps and $n = 14$ from an up-chirp. The estimated beat frequency from a down-chirp coincident with $f_{b_up}(14)$ would be $f_{b_dn}(14^*)$, where

$$f_{b_dn}(14^*) \cong (f_{b_dn}(13) + f_{b_dn}(15))/2. \quad (7)$$

From these two coincident observations a range-dependent beat frequency is then obtained as

$$f_{b_up}(14) - f_{b_dn}(14^*) \cong f_{R_up}(14) - f_{R_dn}(14^*) \quad (8)$$

$$f_{R_up}(14) - f_{R_dn}(14^*) = 4BR(14)/(\tau c) \quad (9)$$

such that

$$R(14) \cong \{f_{b_up}(14) - f_{b_dn}(14^*)\}(\tau c/4B) \quad (10)$$

and

$$f_D(14) \cong f_{b_up}(14) - f_o - f_{R_up}(14) \quad (11)$$

$$v(14) \cong -f_D(14) c/(2 f_{RF}). \quad (12)$$

Alternatively, once the object’s entire time-of-flight has been acquired, a post-processing linear analysis of the beat frequency progression can be performed to realize a more accurate determination of range and velocity over this interval, at a higher latency of course. These parameters are denoted as $R(t)$ and $v(t)$, respectively.

These beat frequency analyses are shown in Figs. 12 and 13 for the **fired away** data from Figs. 8 and 9. Results indicate that during the approximately 95 observations (individual up-chirps and down-chirps), which span about 46 ms, the reball’s radial velocity decreases from about 93 m/s (initial observation at a range of 1 m) to a final value of about 85 m/s (at a range of 5.3 m), with an average deceleration rate of

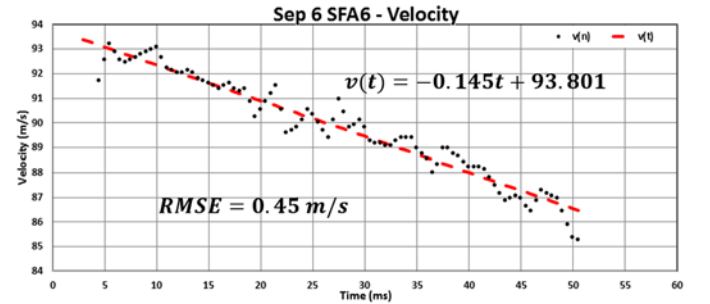


Fig. 12. Plot of estimated reball velocity $v(t)$ overlaid with the low-latency estimate $v(n)$. The equation estimated for $v(t)$ and the corresponding RMS error are also shown.

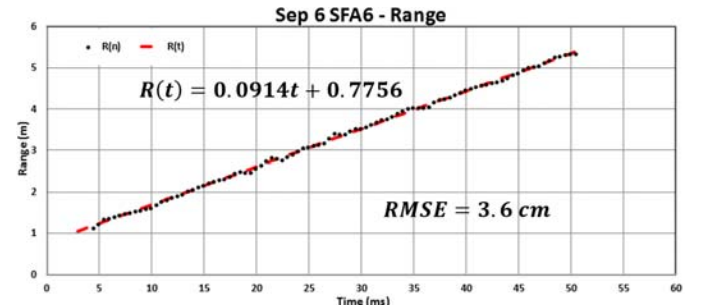


Fig. 13. Plot of estimated reball range $R(t)$ overlaid with the low-latency estimate $R(n)$. The equation estimated for $R(t)$ and the corresponding RMS error are also shown.

about 15 cm/s/ms. Figure 12 shows that the quick estimate of velocity achieves an RMS error less than 0.5 m/s, while the quick range estimate in Fig. 13 realizes an RMS error of 3.6cm.

V. CONCLUSIONS

Millimeter-wave radar systems achieve high Doppler sensitivity that can be exploited to detect and track fast-moving objects. Here a W-band FMCW heterodyne radar was constructed and used to measure a reusable paintball, or reball, during its flight, with the heterodyne attribute permitting isolation of a “clutter only” measurement that facilitates clutter cancellation. In the resulting spectrogram after dechirping the progression of the reball’s changing range and radial velocity can be observed, to the degree permitted by the surrounding clutter.

The combination of an up-chirp and down-chirp can also be used to estimate the range and velocity with high accuracy once the clutter has been adequately suppressed. To cancel clutter in this arrangement, a “fold-and-subtract” technique is employed that is found to reduce the clutter by at least 25 dB, thereby clearly revealing the path of the reball. In a companion paper [8] an adaptive approach is likewise applied to this nonstationary scenario.

VI. ACKNOWLEDGEMENTS

We thank the following people who assisted with this effort: Jeff Redmond for his mechanical work on the radar system assembly; Alex Griffin for automating portions of the radar start-up process and synchronizing the direct digital synthesizers; and Lyndi Hanson for assisting in acquiring the paintball gun and associated hardware from the ROTC program at KU.

VII. REFERENCES

- [1] S. Rahman, D.A. Robertson, “Time-frequency analysis of millimeter-wave radar micro-Doppler data from small UAVs,” *Sensor Signal Processing for Defence Conf.*, London, UK, Dec. 2017.
- [2] E. Hyun, W. Oh, J.-H. Lee, “Detection and tracking algorithm for 77GHz automotive FMCW radar,” *Intl. Asia/Pacific Conf. on SAR*, Seoul, Korea, Nov. 2011.
- [3] H. Rohling, M. Kronauge, “New radar waveform based on a chirp sequence,” *Intl. Radar Conf.*, Lille, France, Oct. 2014.
- [4] E. Hyun, W. Oh, J.-H. Lee, “Two-step moving target detection algorithm for automotive 77 GHz FMCW radar,” *IEEE Vehicular Technology Conf. - Fall*, Ottawa, Canada, Sept. 2010.
- [5] M.-T. Dao, D.-H. Shin, Y.-T. Im, S.-O. Park, “A two sweeping VCO source for heterodyne FMCW radar,” *IEEE Trans. Instrumentation & Measurement*, vol. 62, no. 1, pp. 230-239, Jan 2013.
- [6] Y. Liu, D. Goshi, K. Mai, L. Bui, Y. Shih, “Linearity study of DDS-based W-band FMCW sensor”, *IEEE MTT-S Intl. Microwave Symp. Digest*, no. 4, pp. 1697-1700, June 2009.
- [7] L. Shi, C. Allen, M. Ewing, S. Keshmiri, M. Zakharov, F. Florencio, N. Niakan, R. Knight, “Multichannel sense-and-avoid radar for small UAVs,” *IEEE/AIAA Digital Avionics Systems Conf.*, East Syracuse, NY, Oct. 2013.
- [8] C.C. Jones, L.A. Harnett, C.A. Mohr, S.D. Blunt, C.T. Allen, “Structure-based adaptive radar processing for joint clutter cancellation and moving target estimation,” submitted to *IEEE Intl. Radar Conf.*, Washington, DC, Apr./May 2020.
- [9] <https://www.vadiodes.com/en/compact-receiver-modules-mixamc-i>
- [10] L. Goodman, “W-band FMCW radar for range finding, static clutter suppression & moving target characterization,” Master’s Thesis, University of Kansas, Aug. 2019.